Journal of ELECTRICAL ENGINEERING, VOL. 56, NO. 3-4, 2005, 71–77

BINARY PSK/CPFSK AND MSK BANDPASS MODULATION IDENTIFIER BASED ON THE COMPLEX SHANNON WAVELET TRANSFORM

Radomír Pavlík *

This paper addresses a modulation identification method for three basic bandpass digital modulation schemes under constant envelope class: binary PSK (BPSK), binary continuous-phase FSK (CPBFSK) and MSK using the complex Shannon wavelet transform. This method does not require any restriction on the baseband signal pulse because the recognized signal is considered as bandpass carrier-modulated transmitted over a simulated noisy communication channel. A simple method for determining the mother wavelet parameters is proposed. A threshold based optimum classifier is designed to identify these three modulations buried in additive white Gaussian noise. The classification problem is examined as the classical binary hypothesis test for BPSK/{CPBFSK/MSK} and CPBFSK/MSK sourced hypotheses. The performance of this classifier is expressed in terms of the probability of correct classification for various signal-to-noise power ratios (SNR).

K e y w o r d s: complex Shannon wavelet transform, digital modulations, identification, bandpass signal

1 INTRODUCTION

The identification of digital modulation signals is one of the important features of each sophisticated spectrum monitoring measurement and analysis software system [1, 2]. The signal identification process is an intermediate step between signal interception and demodulation for characterizing signals in various military and civilian communications applications including spectrum management, surveillance, electronic warfare, military threat analysis.

There is already an extensive and diverse unclassified literature devoted to this field. It is therefore impossible to cover it exhaustively, or even relatively so. Several approaches for determining the modulation type and signal parameters focus on extracting signal characteristics under different conditions and it makes difficult (if not impossible) to compare the performance of such methods from disparate sources. Anyway, there are generally two basic approaches to the identification problem: decision-theoretical and statistical pattern recognition. The decision-theoretical approach is based on hypothesis testing for sourced hypotheses conditioned to a finite set of known candidate signals. The pattern recognition approach usually consists of the following steps: i) feature extraction, ii) reduction of the feature space, and iii) classification based on the lower dimension feature space.

One of the basic feature extraction methods, especially when dealing with non-stationary signals, is time-frequency analysis [3], particularly the wavelet transform (WT). Although the WT has been found useful for analyzing signals in both time and frequency in recent research, just a few of unclassified publications on communication signal identification are available in open literature. One of the most complex and important is an identifier introduced by Ho, Prokopiw and Chan [4]. They apply the Haar WT and statistical decision theory to the problem of identification of M-ary phase shift keying (MPSK) and frequency shift keying (MFSK) signals without baseband filtering contaminated by additive white Gaussian noise (AWGN). Unfortunately, this method fails when there is pulse shaping and baseband filtering, which is applied in almost each practical transmission system, so this method is unusable under real conditions.

Therefore in this paper, in order to approximate to a real transmission system, the analysed modulation signal is considered to be bandpass carrier-modulated. The proposed identifier is designed to process three basic modulation types: BPSK, CPBFSK and MSK, and has *a priori* knowledge of the modulation method employed at the transmitter.

In the following sections, a modulation identification concept (Section 2) and a short overview of continuous wavelet transform (CWT) are presented (Section 3). Then the new complex Shannon wavelet approach together with the proposed CWT identification subsystem is introduced (Sections 3.1–5). In Section 4, simulation and experimental results are provided to show the performance of the identification method in the presence of AWGN environment. The paper concludes in Section 5 and with an acknowledgment.

2 MODULATION IDENTIFICATION CONCEPT

As illustrated in Fig. 1, the bandpass modulation identifier consists of two main components: CWT identifica-

* Military Technical Institute of Protection, Veslařská 230, 637 00 Brno, Czech Republic, E-mail: pavlik@vtuo.cz

ISSN 1335-3632

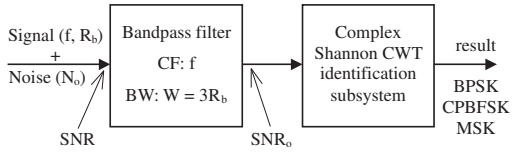

Fig. 1. Bandpass modulation identifier.

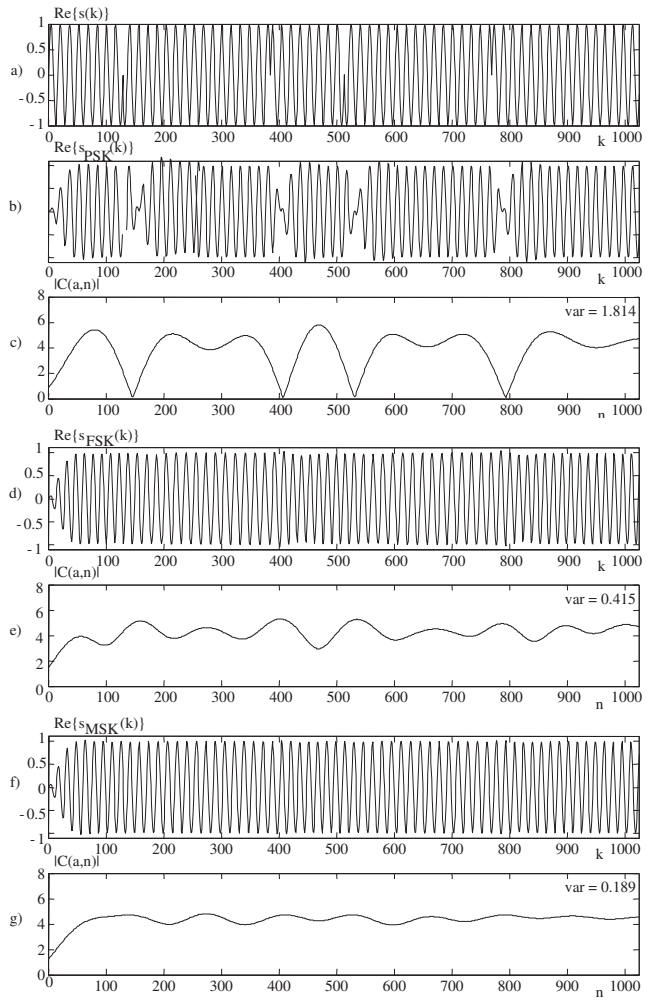

Fig. 2. Modulation waveforms and CWT magnitudes, $a = 16$, $f_c = 1.0$, $f_b = 0.25$, SNR$= \infty$. Modulation waveforms of: a) ideal BPSK, $\Theta = \pi/2$, b) ideal BPSK after passing through an ideal 4th order Butterworth bandpass filter (propagation delay of the filter is not compensated), d) filtered CPBFSK, $\Theta = 0$, f) filtered MSK, $\Theta = 0$; CWT magnitude of filtered: c) BPSK, e) CPBFSK, g) MSK; var denotes variance of $|C(a, n)|$.

tion subsystem, which will be described later, and a narrowband bandpass filter with a frequency response $H(f)$ centred at f. This filter is to reject the out-of-band noise and restrict the frequency band of the signal. Although this filter is primarily intended as a part of the receiver, it should be considered as the overall filtering characteristic of the pulse- shaping filter, amplitude baseband transmitter filter, channel and receiver for analysis purposes.

The signal, together with wideband white Gaussian noise (of one-sided power spectral density N_0), is passed through the bandpass filter of noise-equivalent bandwidth W centred at f. The comparison of the modulation identifier performance for considered digital modulation methods would not be very meaningful, unless it were made on the basis of some constraint, such as a fixed data bit rate of transmission and fixed bandwidth. Therefore the filter bandwidth is set according to the largest null-to-null bandwidth of all the three modulations signals, which is equal to $3R_b$ for continuous-phase FSK (called also *Sunde's FSK*, [5]), where R_b is the data bit rate. Thus the filter bandwidth is set as $W = 3R_b$. We can remark this means the passband spectrum should contain more than 99 % of the power for the FSK and MSK modulation schemes: $B_{99\%} \approx 2.12\, R_b$ (FSK), $B_{99\%} \approx 1.2\, R_b$ (MSK) [5].

The signal-to-noise power ratio at the output of the bandpass filter, SNR_0, is simply the ratio of the bandpass signal power P_0 to the noise power P_n measured at the output of the filter,

$$\mathrm{SNR}_0 = \frac{P_0}{P_n} = \frac{F(\eta) P_s}{N_0 W}\,, \tag{1}$$

where $\eta = W/R_b$ is the normalized input bandwidth and $F(\eta)$, $0 \le F(\eta) \le 1$, is the fraction of the initial passband signal power P_s passing through an ideal filter of noise-equivalent bandwidth (defined for a filter $H(f)$ as $W = \frac{1}{|H(0)|}\int_{-B/2}^{B/2} |H(f)|^2 \mathrm{d}f$, [6]) $W = \eta R_b$ and negligible passband loss. For binary signals, $P_s = P_a/2$, where P_a is the power of the baseband modulating signal. The signal-to-noise power ratio at the input to the bandpass filter, SNR, is then related to SNR_0 by

$$\mathrm{SNR}_0 = F(\eta)\mathrm{SNR}\,. \tag{2}$$

The calculation of $F(\eta)$ for PSK signals is developed in the paper [7] and is used to precisely adjust the requested SNR value.

Within the modulation identifier, at the point following the narrowband input bandpass filter, the input to the CWT identification subsystem is defined as

$$x(t) = s(t) + n(t)\,, \tag{3}$$

where $s(t)$ is the bandpass signal and $n(t)$ is the noise. The signal $s(t)$ can be represented as [6]

$$s(t) = \mathrm{Re}\left[\nu(t) e^{j(2\pi f t + \Theta)}\right]\,, \tag{4}$$

where f is the carrier frequency or the intermediate frequency after down-conversion (if necessary), Θ is the initial carrier phase and $\nu(t)$ is usually called the complex envelope of $s(t)$.

In general, for PSK signal,

$$\nu_{PSK}(t) = A \sum_{k=-\infty}^{\infty} a(t - kT) e^{j\theta_k}\,, \tag{5}$$

where A is the signal amplitude, $a(t)$ is a rectangular pulse with unit amplitude defined on $[0,T]$, T is the symbol period, $\theta_k = 2\pi(m-1)/M$, $m = 1,\ldots,M$, are the M possible phases of the carrier f, $-\infty \le t \le \infty$, and $\Theta = \pi/2$ in this paper.

For CPBFSK signal,

$$\nu_{CPFSK}(t) = A\exp\left[j\Big(\frac{\pi h a_k(t-kT)}{T} + \phi_k\Big)\right], \qquad (6)$$

in the interval $kT \le t \le (k+1)T$, for the kth data bit $a_k = \pm 1$, $k = 1,2$; where $h = 2\Delta f T$ is the modulation index, Δf is the peak frequency deviation, $T = T_b$ is the data bit period, $\phi_k = \pi h \sum_{i=0}^{k-1} a_i$ represents the accumulated phase, which is constant in the bit interval. In the square brackets, the first term represents the linearly changing phase.

For MSK signal, which is a special form of binary CPFSK with the modulation index $h = 1/2$,

$$\nu_{MSK}(t) = A\exp\left[j\Big(\frac{\pi a_k(t-kT)}{2T} + \phi_k\Big)\right], \qquad (7)$$

where $\phi_k = 0$ or π.

Figure 2 shows the BPSK, CPBFSK and MSK signals before and after passing the bandpass filter. It can be seen that transients in the filtered BPSK signal (Fig. 2(b)) are distorted, which corresponds to the real BPSK signal, transmitted through a communication channel.

Since only the BPSK signal shows distinct transients, the goal to differentiate BPSK, CPBFSK and MSK signals was to seek a 'signal-adapted' wavelet, which is 'matched' particularly to BPSK signal or to a class of CPBFSK/MSK signals. An ideal solution would be to use or in the best scenario develop a correspondingly systematic and efficient design algorithm for modulation signal-adapted wavelet bases, which tends to another and uneasy task. In this paper, searching of applicable wavelet (scaling) function was restricting to members of standard wavelet families.

3 CONTINUOUS WAVELET TRANSFORMATION

The continuous wavelet transform of a signal, $s(t)$, is defined as [8]

$$C(a,b) = \int_{-\infty}^{+\infty} s(t)\psi_a^*(t)\mathrm{d}t = \frac{1}{\sqrt{a}}\int_{-\infty}^{+\infty} s(t)\psi^*\Big(\frac{t-b}{a}\Big)\mathrm{d}t, \quad (8)$$

where a is the dilation parameter (scale) of the wavelet, b is the location parameter of the wavelet, $\psi^*(t)$ is the complex conjugate of the wavelet mother function $\psi(t)$. The baby wavelets $\psi_a(t)$ come from time scaling and translation of $\psi(t)$. $C(a,b)$ contains the local frequency information of $s(t)$ at time $t = b$ and frequency $f_a = f_0/a$, where f_0 is the characteristic frequency of $\psi(t)$ defined for scale $a = 1$ and $b = 0$ (note that f_0 is often called also central frequency, peak frequency, passband center frequency, among others).

3.1 Choosing of the wavelet function

A basic analyzing wavelet function to be compared with the signal should be chosen. There are many different functions suitable as wavelets, each one having different characteristics that are more or less appropriate depending on the application. In the MATLAB Wavelet toolbox [9], there exist many kinds of both real and complex wavelets. The possibility of choosing the wavelet function to be compared with the signal is one of the main advantages of wavelets over Fourier-based methods. A basic requirement is that it looks similar to the patterns to be localized in the signal. A naive approach to find a solution to this problem can be done by searching of a function, which would be suitable to approximate both the analysed signal envelope (especially incl. those patterns at bit transitions of the BPSK signal) and frequency content of the signal. This requirement might be satisfied by a composite function of the sinc function, $\mathrm{sinc}(t) = \sin(\pi t)/\pi t$, and a complex sinusoid.

The parameterized sinc function is just the wavelet (scaling) function of *Complex Frequency B-Spline* wavelets defined by [9]

$$\psi(t) = \sqrt{f_b}\left[\mathrm{sinc}\Big(\frac{f_b t}{m}\Big)\right]^m e^{2j\pi f_c t}, \qquad (9)$$

depending on three parameters: m is an integer order parameter, f_b is a bandwidth parameter, and f_c is a wavelet centre frequency.

Generally complex wavelets possess the following properties that can make them optimal and powerful feature detection tools for signal analysis: they have closed expression, compact support and a nearly optimal time-frequency resolution, and are (anti-) symmetric.

In the particular case $m = 1$, the scaling function $\varphi(t)$ simplifies to the classical Shannon scaling function $\varphi(t) = \mathrm{sinc}(t)$ and the obtained family is known as *Complex Shannon wavelets* defined by

$$\psi(t) = \sqrt{f_b}\,\mathrm{sinc}(f_b t)\, e^{2\pi j f_c t}. \qquad (10)$$

The complex Shannon wavelet is simply a set of complex sinusoids within a $\mathrm{sinc}(\cdot)$ function envelope, where the bandwidth parameter, f_b, controls the width of main lobe of $\mathrm{sinc}(\cdot)$ function.

The complex sinusoidal waveform is contained in the term $e^{2\pi j f_c t}$. The sinc function envelope $\mathrm{sinc}(f_b t)$ 'confines' both real and imaginary part of the complex sinusoidal waveform. The imaginary part is phase shifted from the real part by $\pi/4$. The $\sqrt{f_b}$ term is normalization factor, which ensures that the wavelet has unit energy.

The complex Shannon wavelets are shown in Fig. 3 for $f_c = 1.0$. The central frequency, f_c, determines the number of significant oscillations of the complex sinusoid within the lobe of sinc function.

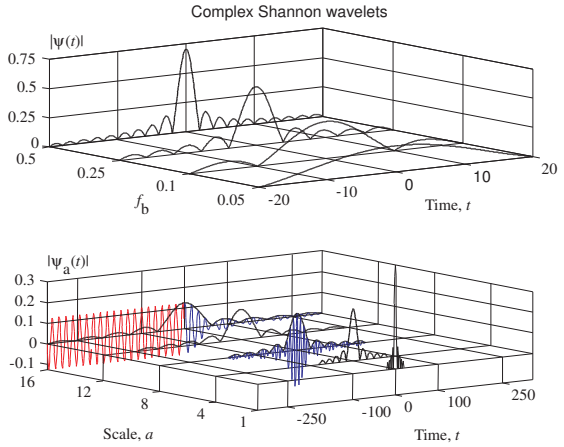

Fig. 3. The set of original (top) and dilated (bottom) Complex Shannon wavelets with effective support of $[-20, 20]$ for: (top) $f_c = 1.0$, (bottom) $f_c = 1.0$, $f_b = 0.25$; real part $\mathrm{Re}\{\psi_a(t)\}$ is plotted for scale $a = 8$, at scale $a = 16$ is simultaneous plot of f_a and $\mathrm{Re}\{\psi_a(t)\}$ on the intervals of $[-320, 0]$ and $[0, 320]$, respectively.

3.2 The application of CWT

Generally, the complex envelope of $s(t)$ in (4) may be expressed for all the three modulation types as

$$\nu(t) = A \exp\big(j\phi(t; \mathbf{a})\big)\,, \tag{11}$$

where $\phi(t; \mathbf{a})$ represents the time-varying phase of the carrier, $\mathbf{a}$ represents all possible values of the information sequence $\{a_k\}$, in the case of binary symbols $a_k = \pm 1$. After substitution of (4) (with $\nu(t)$ based on (11)) and (10) in the equation (8), the resulting integral of $C(a, b)$ is of the form of

$$C(a,b) = \frac{Ae^{(\phi(\cdot)+\Theta)}}{j\sqrt{af_b}} \left[Ei\big(n, y_1\big) - Ei\big(n, y_2\big)\right], \tag{12}$$

where $Ei\big(n, y\big) = \int_1^\infty \exp\big(-yu/u^n\big)\mathrm{d}u$ is the exponential integral, $n = 1$, $y_1 = -jt(2\pi f - 2\pi f_c - f_b)$ and $y_2 = -jt(2\pi f - 2\pi f_c + f_b)$. Expression (12) does not reduce to a simple form (checked using Maple 7) and must be evaluated numerically by taking its absolute value $|C(a, b)|$.

For digital implementation, both the analysed signal and the CWT transform integral computation are discretized at the sampling interval T_s (equal to unity after normalization). Then let $t = kT_s = k$, $b = nT_s = n$, and for a discrete signal $s(k)$, $k = 1, 2, \ldots, N$, where N is number of samples of signal, the eqn. (8) can be redefined as

$$C(a,n) = \frac{1}{\sqrt{a}} \sum_k s(k)\psi^*\Big(\frac{k-n}{a}\Big), \tag{13}$$

where the discretized Complex Shannon wavelets are

$$\frac{1}{\sqrt{a}}\psi\Big(\frac{k}{a}\Big) = \sqrt{\frac{f_b}{a}}\,\mathrm{sinc}\big(f_b k\big)\, e^{j2\pi f_c k}. \tag{14}$$

3.3 A method of calculating f_b and f_c parameters

There is a 'blind' approach in order to find optimal values of all the parameters; one should compute the wavelet transform on a dense sequence of scales using pairs of different values of f_c and f_b. However, some basic assumption can be taken in consideration. First, it is assumed that the low frequency components of the original signal, which correspond to the BPSK signal envelope, will manifest at some maximum scale $a_{\max}$ of given scale levels interval $[a_1, a_{\max}]$ used for CWT analysis. The $a_{\max}$ is fixed for the overall algorithm so this allows to markedly saving computations since we do not need to compute the wavelet transform at any other scale.

Further, looking at both Figs. 2 and 3, it is obvious that the convolution of the filtered BPSK signal with the dilated version of the wavelet function at scale $a_{\max}$ over the bit period T_b is maximized when:

A) the characteristic frequency f_a captures the carrier frequency f. A way to ensure this condition is to satisfy the following simple relationship

$$f_a \equiv f = \frac{F_s f_o}{a} = \frac{F_s f_c}{a}\,, \tag{15}$$

where $a = a_{\max}$, F_s is the sampling rate of mapped modulation signal, f_0 is the characteristic frequency of the mother wavelet, which is equivalent just to the Complex Shannon wavelet centre frequency f_c. Thus, f_c can be computed from (15) for any particular bandpass scheme with f and F_s parameters.

B) and at the same time, the width of the main lobe of sinc function, w, determined by the bandwidth parameter f_b, is matched to the bit period T_b

$$w \equiv T_b = \frac{F_s f_b}{2aF_d}\,. \tag{16}$$

By applying both the above terms, CWT magnitudes are shown in Figs. 3(c,e,g), and the following conclusions can be extracted: For BPSK, when the wavelet lies in the middle of bit interval, the CWT magnitude is maximal. On the other hand when the wavelet coincide with the phase transition, the CWT magnitude is minimal. For binary CPFSK, the behaviour of CWT magnitude is different because the wavelet is unmatched either to CPBFSK lower frequency f_1 or higher f_2. Since MSK is a special case of CPBFSK, the CWT magnitude curve is in shape coincidence with CPBFSK curve but has flatter amplitude behaviour due to the fact that the modulation index $h_{MSK} = {}^1\!/_2 h_{CPBFSK}$, *ie* the two MSK frequencies f_1, f_2 are more closely to the carrier frequency and, therefore, to the wavelet f_a frequency.

Comparing Figs. 3(c,e,f) reveals that BPSK has distinctively higher variance than both CPBFSK and MSK, so these can be distinguished by computing the variance

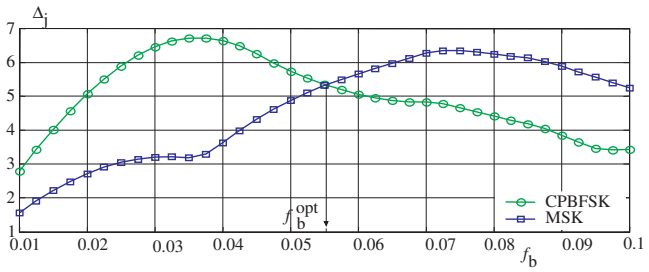

Fig. 4. Determination of an optimal value of the wavelet bandwidth f_b^{opt} as an intersection of variance difference curves.

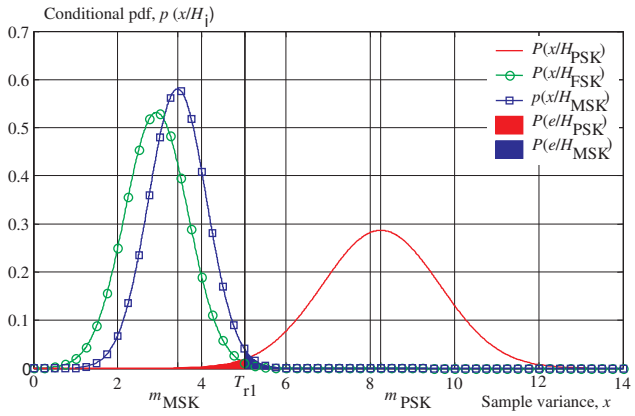

Fig. 5. Conditional probability density functions of sample variance x under hypothesis H_i for the probability of misclassification $P(e/H_i)$.

of the CWT magnitude. The similar approach is used for determining an optimal value of the bandwidth parameter f_b^{opt} because simulation results showed that determining f_b according to B) term may not be optimal with respect to statistical properties of CWT magnitude used as identification criteria (*ie* its variance and mean, see later). In addition, the identifier does have not exact knowledge of T_b. Therefore, once the wavelet centre frequency is obtained, it is proposed to compute the difference between the variance of BPSK and CPBFSK/MSK at scale $a_{\max}$ in the absence of noise (SNR$=\infty$) over f_b

$$\Delta_j = \sigma_{PSK}^2 - \sigma_j^2 \quad j \mapsto \{CPBFSK,\ MSK\}\ , \qquad (17)$$

where $\sigma_u^2 = E\big(|C_u(a,n)|^2\big) - m_u^2$ is the variance of $|C_u(a,n)|$, and set the f_b^{opt} as an intersection point of these two relations. This is illustrated in Fig. 4.

For reaching a decision on which of the modulation signals was transmitted, the relevant statistics can be evaluated under the condition that the transmitted signal is corrupted with AWGN. The proposed method based on the classical binary hypothesis test [10] with determining an optimum decision criterion is described in the following section.

3.4 Case 1: BPSK and CPBFSK/MSK

According to the previous section, the sample variance of the discretized CWT magnitude was proposed as the test statistic

$$x = E\big(|C(a,n)|^2\big) - \big[E\big(|C(a,n)|\big)\big]^2 = \frac{1}{N}\sum_{n=1}^{N}|C(a,n)|^2 - \Big[\frac{1}{N}\sum_{n=0}^{N}|C(a,n)|\Big]^2, \qquad (18)$$

where N is the length of discretized analysed signal and $a = a_{\max}$. Then the classification problem is formulated as a binary hypothesis-testing problem:

H_i: the ith modulation format is assigned to the processed signal,

where i is associated with {BPSK (indexed as $_{PSK}$), j} and j either with CPBFSK (indexed as $_{FSK}$) or MSK, which will be specified later in this section.

Making the statistical decision needs the probability density function (pdf) of the test statistics conditioned on the assigned digitally modulated signal. Assuming the noise in (3) is AWGN, the WT magnitude $C(a,n)$ has a Rician distribution (which is characteristic of random variables generated from linear combinations of sinusoidal signal and a Gaussian noise) [6]. Since the Rician distribution function can be replaced by Rayleigh and Gaussian functions in the noise-only and signal-plus-noise cases, the $C(a,n)$ can be approximated for a wide range of SNR>0 by a Gaussian function. Finally, it can be shown that the pdf of the sample variance (which is a chi-square function) can be well approximated by a Gaussian function, too. Results from MATLAB simulation using the empirical distribution function (*cdfplot* function in MATLAB Statistics Toolbox [10]) confirm this assumption.

The two conditional gaussian pdfs allow a threshold setting to decide between BPSK and CPBFSK/MSK, when a certain probability of false identification of both signals is given. The conditional pdf is

$$p(x/H_i) = \frac{1}{\sqrt{2}\,\pi\sigma_i}\, e^{-(x-m_i)^2/\sigma_i^2}, \qquad (19)$$

and all the three pdfs are shown in Fig. 5, where T_{r1} is the threshold.

Under the hypothesis H_{PSK} is true, the probability of BPSK misclassification is simply the probability that $m_{PSK} - x > m_{PSK} - T_{r1}$, *ie* ,

$$P(e/H_{PSK}) = \int_{-\infty}^{Tr1} p(x/H_{PSK})\mathrm{d}x = \frac{1}{2} + \frac{1}{2}erf\Big(\frac{x - m_{PSK}}{\sqrt{2}\,\sigma_{PSK}}\Big), \qquad (20)$$

where $erf(x)$ is the error function, defined as $erf(x) = 2/\sqrt{\pi}\int_0^x \exp(-t^2)\mathrm{d}t$ [6]. Similarly, if it is assumed that the hypothesis H_j is true, the probability of j signal

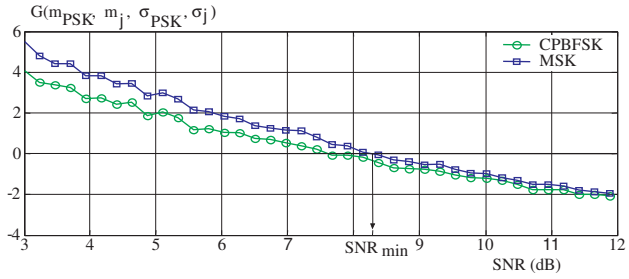

Fig. 6. The left side expression (23) of the condition function (22) versus averaged input SNR.

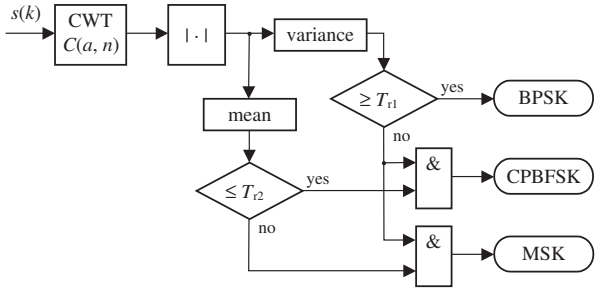

Fig. 7. Complex Shannon CWT identification subsystem.

misclassification is simply the probability that $x - m_j > T_{r1} - m_j$, *ie* ,

$$P\big(e/H_j\big) = \int_{Tr1}^{\infty} p\big(x/H_j\big)\mathrm{d}x = \frac{1}{2} + \frac{1}{2} erf\Big(\frac{m_j - x}{\sqrt{2}\,\sigma_j}\Big), \quad (21)$$

It is obvious when the noise increases the distance between mean values m_{PSK} and m_{FSK} decreases until the point when both the probabilities of misclassification are equal. Thus, $P\big(e/H_{PSK}\big) = P\big(e/H_j\big) = 0.01$ and the condition for setting the optimal threshold value T_{r1} can be obtained

$$G\big(m_{PSK}, m_j, \sigma_{PSK}, \sigma_j\big) = 0\,, \quad (22)$$

where

$$G(\cdot) = 1.6450\sqrt{2}\big(\sigma_{PSK} + \sigma_j\big) + m_j - m_{PSK}\,. \quad (23)$$

Then this relation gives the related threshold value

$$T_{r1} = \frac{m_{PSK}\sigma_j + m_j\sigma_{PSK}}{\sigma_{PSK} + \sigma_j}\,. \quad (24)$$

From the pdfs of CPBFSK and MSK, the one having achieved the condition (22) as the first (with respect to the decreasing SNR value), is selected for the hypothesis test.

The graph of $G(\cdot)$ expressed in (23) as a function of the SNR is shown in Fig. 6. This graph illustrates that this function is a monotonic function of the SNR so that it allows to uniquely determine the minimum SNR, $\mathrm{SNR}_{\min}$, that can satisfy the pre-defined probability of misclassification $P\big(e/H_i\big)$. In this particular case of identification, j is associated with MSK according to the computation of $G(\cdot)$. Hence, $H_j = H_{MSK}$, $m_j = m_{MSK}$ and $\sigma_j = \sigma_{MSK}$ in (21)–(24).

3.5 Case 2: CPBFSK and MSK identification

In this identification arm, the same previously described method is used for setting the related threshold T_{r2} on the understanding that the sample mean was chosen as the test statistic. Sourced hypotheses are associated with {CPBFSK, MSK}. Decision making between CPBFSK and MSK is still conditioned to sample variance thresholding as is shown in Fig. 7 where the block diagram of identification subsystem is presented. This subsystem computes the mean and the variance of the CWT magnitude and compares them with the thresholds T_{r1} and T_{r2}. The decision is based on the following simple rule

$$\begin{aligned} &var \geq T_{r1} \mapsto BPSK\,, \\ &\big(var < T_{r1}\big) \wedge \big(mean > T_{r2}\big) \mapsto CPBFSK\,, \\ &\big(var < T_{r1}\big) \wedge \big(mean \leq T_{r2}\big) \mapsto MSK\,. \end{aligned} \quad (25)$$

It is assumed that the bandpass filter eliminates the *dc* content in the transmitted signal.

4 SIMULATION, RESULTS

A computational implementation of the proposed identifier on MATLAB was developed. Its performance is evaluated as a function of signal-to-noise power ratio SNR for three different modulation type signals: BPSK, CPBFSK and MSK with equal data bit rate $R_b = 1/32f$. Each signal is carried modulated at carrier frequency f to produce a transmitted bandpass signal, which passes through an ideal narrowband 4th order Butterworth bandpass filter of fixed bandwidth $W = 3R_b$, thus $R_b/W < 1$. No other transmission impairments, as well as any form of time dispersion (*ie* signal fading) are considered. The waveforms of modulation signals are generated for a data stream of $n = 16$ symbols with Gray coded bit assignment. The other parameters used are: $F_d = 1$, $F_s = 128$, $f = F_s/16$, $N = 2048$, $h_{CPBFSK} = 1$. In (5) $M = 2$ and $a(t)$ is the rectangular pulse with unit amplitude defined on $[0, T_b]$. Oversampling (number of samples per T_b, equal to F_s/F_d) at 32× was expected to be sufficient. N_0 in (1) was adjusted to achieve the requested input average SNR value computed according to (2) and checked by calculating both the signal (P_0) and noise (P_n) powers at the output of the bandpass filter.

The first step is setting of the unknown threshold values. Their computation is derived for the two binary hypotheses tests with a 0.01 probability of misclassification of each the modulated signal, in two experiments. The first one computes the left side expression (23) of the

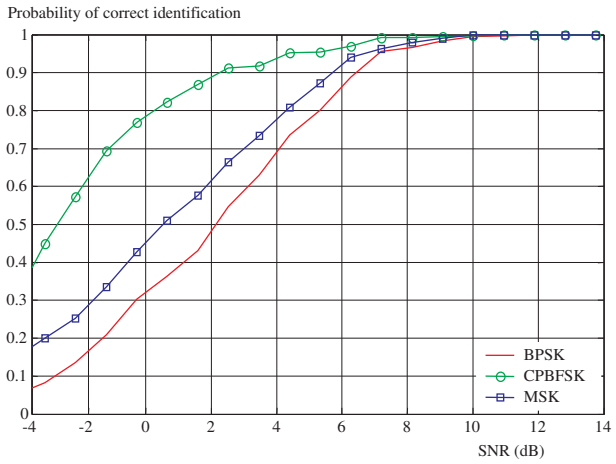

Fig. 8. Identification performance as probability of correct identification versus averaged SNR at the input of bandpass filter for $f_c = 1.0\,,\ f_b = f_b^{opt} = 0.055\,.$

Table 1.

Identification branch	Threshold	$SNR_{\min}$
BPSK/{CPBFSK/MSK}	$T_{r1} = 5.02$	8.25
CPBFSK/MSK	$T_{r2} = 4.88$	−0.20

condition function (22) of the BPSK/CPBFSK identifier and then the related threshold T_{r1} can be computed from (24). The second one computes the (22) and threshold T_{r2} of the CPBFSK/MSK identifier. Identification performance was obtained based on 1000 independent trials and is measured in terms of probability of correct classification. Figure 8 shows its average value measured at the output of the identification subsystem versus the average input SNR for all the three modulation signals. Table 1 summarizes the threshold and related minimum SNR values for: $f_c = 1.0\,,\ f_b = f_b^{opt} = 0.055\,,\ a_{\max} = 16\,,\ \eta = 3\,,$ $F(3) = 0.931$ for BPSK and ≈ 1 for CPBFSK/MSK $(B_{99\%} < W)\,,\ P_s = 0.5\ (A = 1)\,,\ P(e/H_j) = 0.01\,.$

It is clear that CPBFSK and MSK have a slightly higher chance of correct identification. A ~ 1 dB SNR degradation occurs in BPSK signal case comparing to CPBFSK signals to attain an average probability of correct classification of 0.95.

5 CONCLUSION

In this paper, a bandpass modulation identifier using Complex Shannon wavelets was proposed. In order to approximate a practical transmission channel, the effect of bandpass pulse shaping and filtering was considered. This is usually omitted in study the performance of most the published classificators.

The computation speeding of the CWT can be achieved by expressing the (8) formula in Fourier space and performing the computation using an FFT algorithm.

It was shown experimentally that the proposed method works reliably in SNR values greater than $\sim$ 9 dB and its performance does not depend either on the number of symbols that are used to identification or phase/frequency change instants of used modulation signals. Although this paper was focused primarily on the identification of binary modulation signals under constant envelope class, the same or slightly modified method might be useful in the identification of other modulation types under non-constant envelope class (such as the ASK, QAM), as well as of non-continuous FSK and multiple signals. The current research activity of the author is focused on this area.

Acknowledgment

I would like to thank to Professor Andrej Lúč for beneficial discussion on the conception of the bandpass simulation and for his very careful reading of this article.

References

[1] AN-SR-8: Spectrum Explorer: Automatic Modulation Recognition (AMR) Software, Application Note, Interactive Circuits & Systems Ltd., Ottawa, November 2002.

[2] PROCEED S20: HF-Classifier-Demodulator-Decoder, Application Note, Procitec GmbH, Pforzheim, September 2003.

[3] KETTERER, H.—JONDRAL, F.—COSTA, A. H.: Classification of Modulation Modes Using Time-Frequency Methods, 1999 IEEE International Conference on Acoustics, Speech, and Signal Processing, Vol. 5, 1999,.

[4] HO, K. C.—PROKOPIW, W.—CHAN, Y. T.: Modulation Identification of Digital Signals by the Wavelet Transform, IEE Proceedings - F, Radar, Sonar and Navigation **147** No. 4 (2000), 169–176.

[5] XIONG, F.: Digital Modulation Techniques, Artech House, Inc., Norwood, 2000.

[6] PROAKIS, J. G.: Digital Communications, Third Edition, McGraw-Hill, Inc., New York, 1995.

[7] HILL, D. A.—BODIE, J. B.: Carrier Detection of PSK Signals, IEEE Transactions On Communications **49** No. 3 (2001), 487–495.

[8] ADDISON, P. S.—WATSON, J. N.—FENG, T.: Low-Oscillation Complex Wavelets, The Journal of Sound and Vibration **254** No. 4 (2002), 733–762.

[9] MISITI, M.—MISITI, Y.—OPPENHEIM, G.—POGGI, J.-M.: Wavelet Toolbox User's Guide (Version 2.1), The MathWorks, Inc., Natick, 2001.

[10] Statistics Toolbox User's Guide (Version 3), The MathWorks, Inc., Natick, 2001.

Received 26 August 2004

Radomír Pavlík (Ing) was born in Nový Jičín, Czech Republic, in 1974. He graduated from the Faculty of Electrical Engineering and Information Technology, University of Technology, Brno, in 1999. Since 2001 he has worked at the Military Technical Institute of Protection, Brno. At present, he is an external PhD student in the Department of Special Communication Systems at the University of Defence, Brno. His research interest lies in digital signal processing, digital communications and detection/identification of digitally modulated signals.